Variable Optical Delay Line using Discrete Harmonic Oscillation in Waveguide Lattices

Tenghao Li, Qingming Chen, Yunfeng Xiao and Xuming Zhang

Abstract—**This paper proposes a variable optical delay line based on the discrete harmonic oscillation in the waveguide lattice with a quadratic distribution of coupling coefficients. Theoretical analysis and numerical simulation have shown that the device design can achieve a time delay up to 10 ns, with the resolution of 0.5 ns and the 3-dB bandwidth over the whole C-band. It allows a data packet up to 17 bits at the rate of 100 Gbps. In this design, the propagation path is folded by up to 5 times (or 10 times for the one-port design). Compared with the conventional fiber-delay-line buffer, this design has a small footprint (about 10 mm × 0.5 mm). A group of them can be paralleled and cascaded within a small area (e.g., 20 copies into 1 cm^2) as enabled by the microfabrication. With further optimization, this design is potential for interconnecting and signal processing applications in optical communications and computing.**

Index Terms—**Optical buffers, optical delay lines, optical planar waveguide components, optical propagation in anisotropic media, optical computing.**

I. Introduction

Variable optical delay lines (ODLs), or optical buffers, are one of the basic building blocks of the rapidly developing all-optical networks. Nowadays the data traffic is calling for the capacity beyond 100 Gbps [1] and thus motivates the further development of ODL technology. It is still difficult for the current ODLs to reach the data capacity (e.g., 10Gb) as large as their electronic counterparts within the same footprint [2]. However, a capacity of 20 packets with 40 bytes is sufficient for the ODLs to be feasible in backbone internet routers [2].

The existing techniques of ODLs are mostly realized by either increasing the propagation length (delay-line buffer, etc.) or decreasing the group velocity (slow-light buffer, etc.) [3], [4]. The slow-light ODLs are often based on strong resonant effects in photonic crystals and coupled resonator structures [5]–[9]. However, the resonant effect imposes a fundamental limit on the bandwidth. Thus the delay-bandwidth product, a common criterion for evaluation [5], is limited to the order of unity [10], [11]. With a reasonable bandwidth (e.g., > 1 nm), the delay time is usually limited to < 1 ns. Recently, dynamic tuning has been proposed to break the limit by dynamically toggling the cavity between the "closed" and the "open" state [11]–[13], where the light pulses are trapped or released respectively. There are various tuning mechanisms, such as white light cavity effect [11], resonance wavelength shifting [12], and asymmetric cavity-waveguide coupling [13]. The time delay can be significantly extended but at the cost of power consumption and data capacity [5].

In term of the delay-line buffer, the recirculating optical buffer has been developed to use an optical switch to control between the states of storage and transmission [14], [15]. It avoids the trade-off between the bandwidth and the delay, but still has to deal with the contradiction of footprint and loss. In the ODLs that use the optical fibers as the waveguides, the material loss is small but the bending loss prevents small footprint. In the ODLs that use the planar waveguides, the microfabrication enables small footprint and easy integration [14]. However, advanced fabrication is needed to alleviate the side-effects such as strong scattering loss [16]. Other non-resonant ODLs have also been presented, e.g., the traveling wave cavity on a birefringent planar platform [17].

Here we will present a novel idea to realize the ODL using the waveguide lattice (WL). Recent studies have demonstrated the use of WLs for beam steering and routing [18], [19]. When the WLs have a quadratic distribution of coupling coefficients (QWL), the light launched into a single waveguide would wind up and down in the course of forward propagation (see Fig. 1), increasing effectively the propagation length. This effect is called discrete harmonic oscillation (DHO) [20]–[24]. Besides the theoretical research and device design, the experiment observation of DHO is also explored and reported [23]. In other WLs that have linearly varying propagation constants, the optical Bloch oscillation effect is presented [24], [25]. The transition between the Dipole oscillation and the Bloch oscillation is also studied and demonstrated [26]. Some other effects can also be realized by engineering the refractive index of WLs. This raises great interest in the theoretical and experimental studies [26]–[29]. In principle, the QWL-based ODL is similar to the delay-line based ODL, replacing the direct fiber or waveguide ODL with the QWL. By applying the DHO effect, the footprint of ODL device can be shrunk without inducing the bending loss. And the merit of broad bandwidth is also maintained as the DHO is not a resonant effect and the coupling coefficient generally exhibits a low dispersion.

The concept and principle of QWL-based ODL will be elaborated in Section 2, and the device design and the theory

will be given in Section 3. Then, simulation results will be present in Section 4. Finally, the practical issues for realization of the proposed device will be discussed in Section 5.

II. CONCEPT AND PRINCIPLE

The conceptual design of the proposed ODL is shown in Fig. 1a. The light coupled into one waveguide of a WL does not move forward straightly. Instead, it winds up and down periodically in the course of forward propagation (i.e., the DHO effect). This would increase the effective propagation distance when the waveguide length is fixed. It is noted that two conditions are important for the perfect realization of DHO effect, namely the same propagation constant of each single waveguide, and the quadratic distribution of coupling coefficients. Therefore, each waveguide in the WL is made identical, while the distances between the adjacent waveguides are designed to follow a quadratic distribution [20] as,

$$\kappa_m^2 = \left(\gamma/2\right)^2 m\left(M - m\right), \tag{1}$$

in which κ_m denotes the coupling coefficient between Waveguide m and Waveguide $m+1$, with $m = 1, 2, …, M$, here M is the number of waveguides in the WL. Constant γ is the spatial frequency of oscillation by $\gamma = 2\pi/z = 2\pi/(z_s + z_i)$, here z_s and z_i are the lengths of the signal segment and the idle segment in a spatial period z of oscillation, respectively (see Fig. 1b).
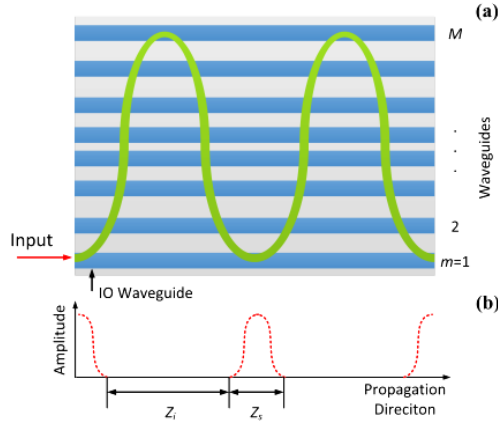

Fig. 1. Discrete harmonic oscillation effect in the QWL (blue regions for the cores and gray for the claddings). The beam (red line) is injected into the system through the bottom waveguide, and goes through a sinusoidal path when propagating from right to left.

When only the waveguide at the bottom (called input-output waveguide, or IO waveguide in short) is excited, the DHO effect would occur [20], [21], and thus the light distribution along the IO waveguide would fluctuate periodically as sketched in Fig. 1(b). In each period, only a short segment of the waveguide has the optical field (the region z_s in Fig. 1b), leaving the other part idle with zero field. The duty cycle D is

$$D = \frac{z_s}{z_s + z_i}. \tag{2}$$

It can be seen from Fig. 1a that the DHO effect in the QWL can be directly used to confine the optical signal in the non-IO waveguides, both spatially and temporally. By tailoring the waveguide length and/or the oscillation frequency, the beam power can be fully delivered to the non-IO waveguides.

III. DESIGN AND THEORY

The DHO in the QWL has usually a long spatial period (e.g., 50 mm), it would be difficult to obtain a large range of time delay in a small footprint. To reduce the waveguide length, we design the QWL-based ODL as shown in Fig. 2. Two parallel high reflection (HR) mirrors are equipped to fold the propagation path of direct QWL in the horizontal direction. For the non-IO waveguides, the HR mirrors are fixed; while for the IO waveguide, the HR mirrors (called shutter mirrors hereafter) can be switched on and off, in other words, between the HR mode and the transmission mode.
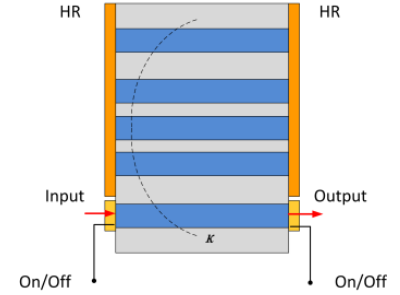

Fig. 2. Schematic design of the QWL-based ODL that uses two fixed parallel HR mirror to fold up the optical path in the horizontal direction so as to reduce the length of waveguide (blue regions). The optical beam (red line) is input into and output from the IO waveguide by two shutter mirrors.
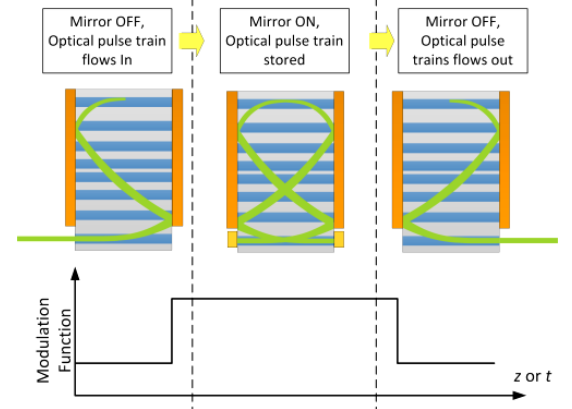

Fig. 3. The flow chart of operation procedures and the sequence diagram of modulation signal.

The operation of QWL-based ODL consists of three main stages: *input*, *storage* and *output*. The flow chart of operation procedure and the sequence diagram of modulation signal are presented in Fig. 3. On the input stage, the shutter mirrors are switched to the transmission mode, and an optical pulse train can be launched into the IO waveguide (see Fig. 3). The optical pulse train may contain multiple bits of data, whose maximum volume is determined by the data rate and the temporal oscillation period. Before the completion of the first oscillation period, the shutter mirrors are switched to the HR mode, and the optical pulse train is totally confined inside the mirror pair (see Fig. 3). After delaying for the desired oscillation periods, the shutter mirrors are toggled off again, and the optical pulse train can exit from the IO waveguide on the output stage (see Fig. 3). From the operation procedure, it can be seen that the time delay resolution is two times of the temporal oscillation periods.

The coupled mode theory [13], [30] is used to analyze the

QWL-based ODL. In the QWLs, the governing equation of wave propagation for the mth waveguide is

$$j\frac{dA_m}{dz} = (\beta_0 + M_l)A_m + \kappa_m A_{m+1} + \kappa_{m-1}A_{m-1}, \tag{3}$$

where $A_m = a_m(z)\cdot\exp(-j\beta_0 z)$ is the amplitude of the mth waveguide mode $\varepsilon_m(x, y)$, and the total field can be formulated as the superposition of the waveguide modes as

$$\varepsilon(x, y) = \sum_{m=1}^{M} A_m \varepsilon_m(x, y). \tag{4}$$

In Eq. (3), the propagation constant β_0 is assumed to be the same for all the waveguides, and the self-coupling coefficient M_l is neglected in the discussions here.

In the matrix form, the governing equations becomes

$$\frac{d\mathbf{A}}{dz} = \mathbf{CA}, \tag{5}$$

in which the amplitude vector $\mathbf{A}$ is constructed by stacking A_m, and the coupling matrix is in tri-diagonal form as given by

$$\mathbf{C} = -i \begin{pmatrix} \beta_0 & \kappa_1 & 0 & 0 & \cdots & 0 & 0 \\ \kappa_1 & \beta_0 & \kappa_2 & 0 & \cdots & 0 & 0 \\ \vdots & \vdots & \vdots & \vdots & \vdots & \vdots & \vdots \\ 0 & 0 & \cdots & 0 & \kappa_{M-2} & \beta_0 & \kappa_{M-1} \\ 0 & 0 & \cdots & 0 & 0 & \kappa_{M-1} & \beta_0 \end{pmatrix}. \tag{6}$$

By solving the matrix equations, the relationship between the amplitudes at distance z and z_0 can be formulated using the matrix exponential as

$$\mathbf{A}(z) = e^{\mathbf{C}(z-z_0)}\mathbf{A}(z_0). \tag{7}$$

In addition, the boundary conditions, which accounts for the shutter mirrors for the IO waveguide, should be applied as,

$$A_1(z_0^+) = M(z_0^-)A_1(z_0^-), \quad z_0 = L, \ 2L, \cdots, \tag{8}$$

where $M(z)$ is the modulation function which takes values 0 or 1 in the simplest case, and L is the length between the mirror pair [27]. The superscripts $+$ and $-$ denote the one-sided limits.

It is simple and helpful to design the QWL-based ODL by using Eqs. (6), (7) and (8), though it unfolds the zigzag propagation path inside the mirror pair. For simple notation, such an analysis is called direct propagation method (DPM).

IV. ANALYTICAL DATA

In this section, simulations based on the DPM are first carried out by the transfer matrix method (TMM) [26], [30], [31]. As mentioned above, the DPM can be used to design and analyze the QWL-based ODLs. Then, the well-developed time-domain transfer matrix method (TD-TMM) method [32]– [34] is also applied to the simulations, which is more rigorous and straightforward.

The simulations are performed by Mathematica. As shown in Eq. (7), the matrix exponential is calculated using the built-in functions. The discretized steps in length or time in both methods induce some numerical error, which scales near linearly with the number of step. Through calculations, it is seen that the numerical error can be neglected even for the following TD-TMM cases.

A. Device design for simulation

With the proposed design in Fig. 2, a sample device is presented for the simulation. The materials are pure silica for the cladding regions and doped silica for the core regions. The parameters and the corresponding values are listed in Table I.

TABLE I
PARAMETERS OF DEVICE DESIGN FOR SIMULATION

Parameter	Value
Length of waveguide	10 mm
Number of waveguide	25
Oscillation spatial frequency γ	0.04π mm^{-1}
Effective refractive index n_{eff} @1550 nm	1.44328

TABLE II
COEFFICIENTS IN SELLMEIER'S FORMULA [30]

	Pure silica	B$_2$O$_3$-doped silica (5.2 mole %)
a_1	0.004679148	0.004981838
a_2	0.01351206	0.01375664
a_3	97.93400	97.93353
b_1	0.6961663	0.6910021
b_2	0.4079426	0.4022430
b_3	0.8974794	0.9439644

In the first part of simulation, only the single wavelength of 1550 nm is considered. In the second part, the device performance over a broad wavelength region of C-Band (1530 – 1565 nm) are computed and compared. In this case, the material dispersion is one of the most important factors, and the difference in refractive indices results in a variation of the coupling coefficients. The material dispersion at wavelength λ is determined by the Sellmeier's formula as [35]

$$n^2(\lambda) = 1 + \frac{b_1\lambda^2}{\lambda^2 - a_1} + \frac{b_2\lambda^2}{\lambda^2 - a_2} + \frac{b_3\lambda^2}{\lambda^2 - a_3}, \tag{9}$$

with the coefficients as listed in Table II for both pure silica and the B$_2$O$_3$-doped silica (5.2 mole %).

To simulate different index contrasts, a coefficient C_{doped} is defined to represent the influence of doping concentration. And the refractive index for B$_2$O$_3$-doped silica with the specific doping concentration is formulated as

$$n_{doped}(\lambda) = n_{pure}(\lambda) + C_{doped}$$
$$[n_{doped-5.2}(\lambda) - n_{pure}(\lambda)], \tag{10}$$

in which the subscript $doped$ and $doped$-5.2 stand for the B$_2$O$_3$-doped silica with the specific doping concentration and with the 5.2 mole % concentration, respectively, and the subscript $pure$ denotes pure silica.

The slab waveguide model is used to calculate the coupling coefficients for different refractive indices and different gap distances between the adjacent waveguides [36]. The width of waveguide is kept at 6μm, and the index difference between the core and the cladding is set at $C_{doped} = 0.25$. The distances between the adjacent waveguides are designed at wavelength of 1550 nm to meet the requirement of quadratic distribution of coupling coefficients (see Eq. (1) and Fig. 4) and the oscillation spatial frequency specified in Table I. For the other wavelengths, the gap distances remain the same as those at 1550 nm, and the coupling coefficients are computed accordingly for the simulation.

In the simulation, the gap distances between the adjacent waveguides are calculated using the above procedure, and the results are shown in Fig. 4. The gap is the smallest (4 μm) in the central region and goes up to 12 μm near the edges. Correspondingly, the coupling coefficient is the highest (0.0008 μm^{-1}) in the central region and drops down quadratically to 0.0003 μm^{-1} near the edges.
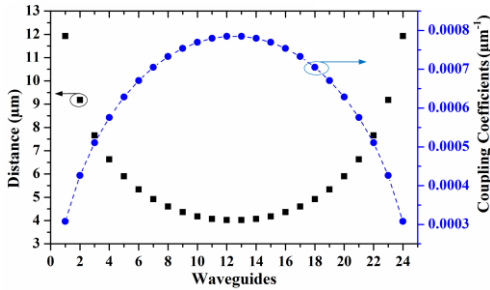

Fig. 4. Gap distances and coupling coefficients between the adjacent waveguides in the simulation.

B. Simulations using DPM and TD-TMM at 1550 nm

The simulations at single wavelength of 1550 nm are performed using both the DPM and the TD-TMM. As discussed above, the DPM can be used as the direct design and analysis method for the proposed device, while the TD-TMM is rigorous and can be used to verify the design.

The targeted time delay is 0.481 ns, which corresponds to the propagation length of 100 mm, though the physical length of waveguide is only 10 mm. The modulation function for the shutter mirrors is depicted in Fig. 5. For time 0 to 0.173 ns, the shutter mirror has 0 reflectivity (i.e., full transmission) to allow the input of optical pulse trains (assuming the rise time is negligible). Then the shutter mirrors are switched to full reflection for a duration of 0.481 ns before they are finally switched to the transmission mode again for the output of optical signals.
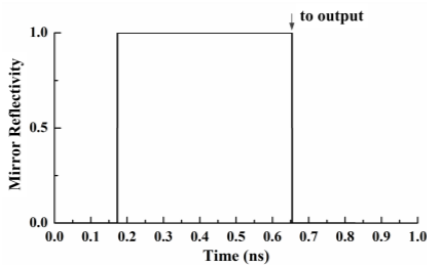

Fig. 5. Modulation function for the shutter mirrors.

Using the DPM, the amplitude distribution along the IO waveguide at 1550 nm is presented in Fig. 6. It can be seen that the oscillation spatial period is 50 mm, which is consistent with the designed oscillation spatial frequency 0.04π mm^{-1}. After three oscillation periods, nearly all the beam power goes out at the distance of 150 mm, showing 15 folds of the waveguide length 10 mm (see Table I). To fully demonstrate the field propagation, the amplitude distributions along all the waveguides are plotted in Fig. 7, showing clearly the DHO effect in the OWLs.
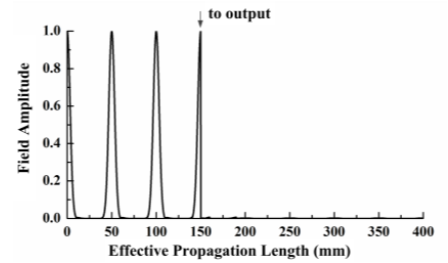

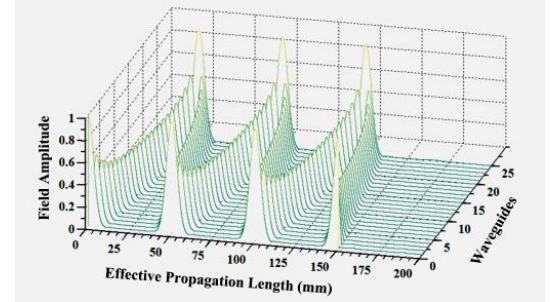Fig. 6. Distribution of the field amplitude along the IO waveguide.

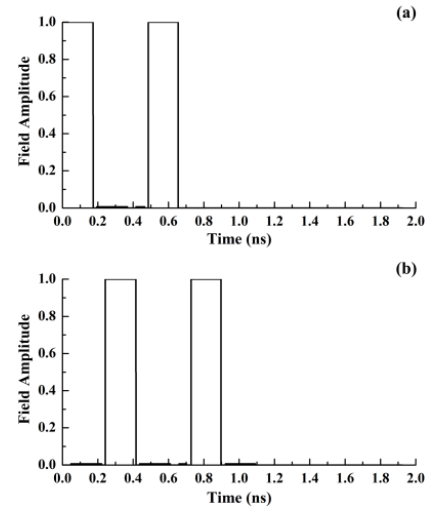Fig. 7. Amplitude distribution along different waveguides.

Fig. 8. Temporal waveforms of the forward-propagating field amplitudes as measured at (a) the input end and (b) the output end of the IO waveguide.

The simulation results using the TD-TMM are presented below. Fig. 8 plots the temporal waveforms of the forward-propagating fields (not including the back-propagating fields) measured at the input end and the output end of the IO waveguide, respectively. On the input side (see Fig. 8a), the field amplitude = 1 initially lasts for 0.173 ns, corresponding to the time range for inputting the optical pulse train. After the shutter mirrors is switched to the HR mode, the light field oscillates between the input and the output end for one round. Finally, at time 0.654 ns the light field exits the IO waveguide, with the amplitude of approximately 1. It is noted that the input-output response is nearly 1 during the time span of 0.173 ns. Therefore, the maximum number of delayed optical pulses can be 17 bits for the data rate of 100 Gbps, or 170 bits for 1000 Gbps. However, when the dispersion effect is considered, the maximum allowed date rate is limited by the pulse distortion. Such an effect will be simulated in next subsection.

The spatial-temporal distributions of forward-propagating field along the IO waveguide are shown in Fig. 9. The temporal

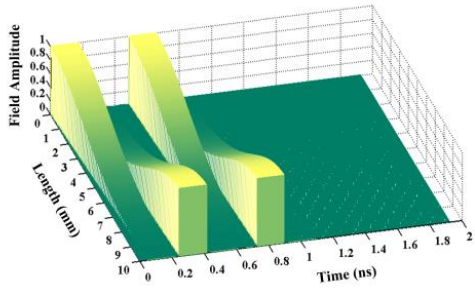propagation of the field matches well with the design target.

Fig. 9. Spatial-temporal distribution of the forward-propagating field along the IO waveguide.

From the simulation results above, it is seen that DPM and TD-TMM are consistent with each other. The TD-TMM simulation provides more information on the spatial-temporal propagation of the field, whereas the DPM is much more computationally efficient and can serve as a quick guide for the device design.

C. Simulations of broadband performance

In term of the broadband performance, the field propagation is first simulated using the DPM and the TD-TMM, at two typical wavelengths of 1542 nm and 1558 nm. The delayed time is designed to be 20 times of the delay time resolution (0.481ns as aforementioned), or approximately 10 ns.
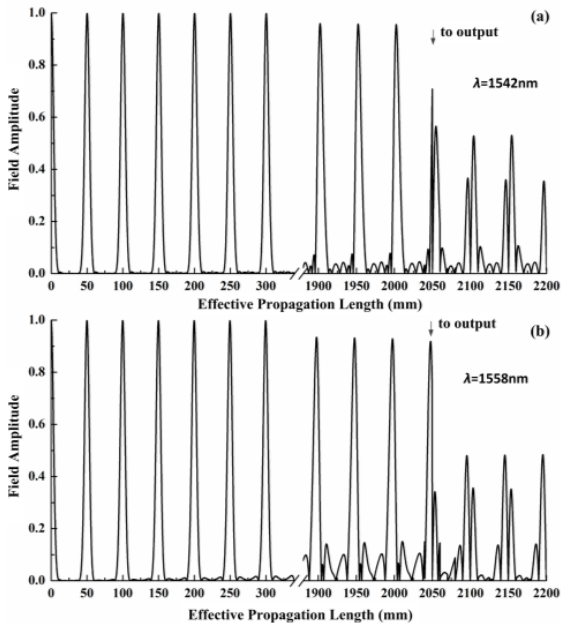

Fig. 10. Amplitude distributions along the IO waveguide at wavelength of (a) 1542 nm and (b) 1558 nm.

Using the DPM, the amplitude distributions along the IO waveguide are shown in Fig. 10. Three features can be observed in the field propagation. The first is that noisy sidebands appear next to each main pulse, and they become severer with the increase of propagation length, unlike the clean pulses in Fig. 6. The second is that even after the shutter mirrors are switched for output, there are still some residual field in the IO waveguides. This is clearly different from those at 1550 nm, i.e., the field amplitude has no residual after the output time point (see Fig. 6). The third feature is that the oscillation

frequency varies with the wavelength (> 50 mm for 1542 mm, and < 50 mm for 1558 nm). All of them are attributed to the deviation of coupling coefficient distribution from the ideal quadratic one, and causes the attenuation of output power and the occurrences of residual/noise. At the two selected wavelengths (1542 nm and 1558 nm) and the delay time 10 ns, the output is attenuated by a factor of approximately 0.75 in amplitude, or slightly above 3 dB in optical power.
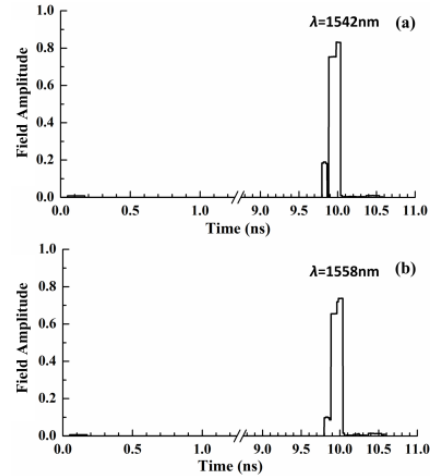

Fig. 11. Temporal waveforms of the forward-propagating field as measured at the output end of the IO waveguide. Two typical wavelengths are considered, namely (a) 1542 nm, and (b) 1558 nm.

Similar results can be obtained by using the TD-TMM. The temporal waveforms of forward-propagating field as measured at the output end of IO waveguide are presented in Fig. 11. It is noted that there are small amount of sudden increase at about 10.0 ns. It is because some portion of energy exists in the backward-propagating field before the mirrors are toggled off. As to the small peaks that occur earlier, they are leakage from the sidebands of main pulses (see Fig. 10) and the variation of oscillation frequency.

To investigate the dispersion over the C-band, the DPM is used to calculate the field amplitudes at the output end of the IO waveguide at different wavelengths, as shown in Fig. 12. The delay time is chosen to be 10 times of the delay time resolution (0.481 ns as mentioned above), or approximately 5 ns. It can be seen from Fig. 12 that the attenuation of amplitude stays below 3 dB over the whole C-band.

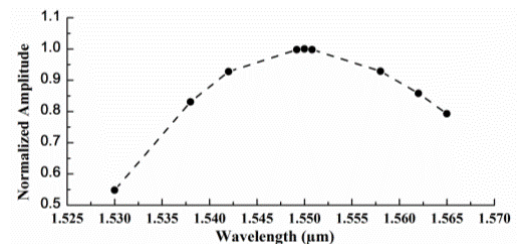Fig. 12 Field amplitudes at the output end of the IO waveguide when the wavelength is varied over the whole C-band.

From the analysis above, the results from the TD-TMM simulations and the dispersion curve provided by the DPM simulations can be used to examine the pulse shape in wave propagation. Linear phase shift is expected across different wavelengths because of the low dispersion characteristic.

Although the TMM and the TD-TMM frameworks are not strictly of full wave nature, the slow-varying temporal modulation is satisfied thanks to the large bandwidth with low dispersion, and they generally work well. For more rigorous analysis on the pulse propagation, more complicated methods may be applied, such as the dispersive FDTD simulation [37]. As the design guidance and performance evaluation, the TMM and the TD-TMM methods are easier and faster, which is a good balance between the accuracy and the computational load.

V. DISCUSSIONS

Here are more discussions on the principle, the performance and the realization of QWL-based ODLs. It is noted that our design looks similar in appearance to the reported Fabry-Pérot resonator arrays [30], which belongs to the family of coupled resonant optical waveguide (CROW) and exhibits the slow light effect. In contrast, our design of QWL-based ODL utilizes traveling wave and is fundamentally different from the standing wave field in the Fabry-Pérot resonator arrays.

In principle, our design can be considered as the extension of delay-line buffer, where the optical fiber is replaced by the QWL. With the QWL, the light propagation path is folded along the propagation direction, and the bending loss in the optical fiber case is eliminated. As a result, the proposed device is more compact. In the vertical direction, 25 waveguides needs a height of only about 0.5 mm. It can be seen that 20 groups of the proposed devices can be integrated within the footprint of 1cm². When the output and the input end are combined (i.e., use only one port for both input and output), only one shutter mirror is needed, and the propagation path can be folded by 10 times. However, a circulator should be used to separate the input and the output pulses. Generally speaking, the proposed device is not as compact as the reported CROW devices [6], [13]. However, when the characteristics of both broad bandwidth and large time delay are needed, the proposed ODL has a comparable footprint with the CROW devices.

The main obstacle for further miniaturization of our design is that the DHO cannot be arbitrarily large, and the occupied length z_s is finite. The duty cycle becomes larger with the increase of waveguide number M, but tends to saturate when M becomes large. Besides, the available value of M is limited as imposed by the quadratic distribution of coupling coefficient. Otherwise, large number of waveguides leads to the requirement of high coupling coefficients that are not physical.

The maximum time delay is limited by the loss and the dispersion in our design. For the propagation loss, both the optical loss of each waveguide and the scattering loss at the mirror should be considered. The optical loss can be suppressed by using silica material which is common in low-loss fiber optics. However, to help fine tune the device after the fabrication, electro-optic or thermo-optic materials are more favorable. A possible solution is to use the silica for the waveguide core, while using the tunable material as the waveguide cladding. The use of electro-optic or thermo-optic materials can also enhance the tunability of the device. However, the relationship between the refractive index configuration and the resulted coupling coefficient is not simply linear and thus needs careful design. On the other hand, the dispersion should be compensated to alleviate the sidebands, the residual noises and the oscillation frequency variation. To relieve the impact of material dispersion, the second-order dispersion coefficients should be chosen carefully. As shown in the simulations, the dispersion of effective index has only mild effect on the modulation function and can thus be neglected.

To lengthen the capacity of data bits, the switch speed of the shutter mirror should be as fast as possible. A possible solution is to utilize a gate matrix switch [14]. Bending loss and scattering loss in each waveguide can be neglected. Moreover, high reflectivity is favorable for the mirrors, since the scattering loss of mirrors is accumulated during the multiple round trips with the increase of delay time. For loss compensation, less compensation amount is needed per round trip due to the folded path, when compared to the recirculating loop buffers [14]. At the mirror-QWL interface, each single waveguide experiences the same phase shift, which can be eliminated as a whole and will not contribute to the pulse shape distortion at the boundary.

There is another contradiction between the maximum data bit and the delay time resolution, which is common for the delay-line optical buffers. To achieve larger data capacity without increasing the delay resolution, faster data rate or larger bandwidth should be applied. As mentioned above, this restriction is alleviated in our design.

Similar to the DHO, the optical Bloch oscillation effect in the WLs with linear effective index can also be applied to realize the ODL. However, the input beam should occupy several waveguides instead of a single one. For the practical realization, the linear tuning of refractive indices is simpler and easier. Therefore, the optical Bloch oscillation may become a competitive alternative to the DHO in the QWL-based ODLs.

VI. CONCLUSIONS

In conclusions, a unique design of optical delay line is proposed by using the discrete oscillation effect in waveguide lattices. The analyses show that the device design can achieve a time delay as long as 10 ns, with the delay time resolution of 0.5 ns. The 3dB-bandwidth spans over the whole C-band for the delay of 5 ns. The data capacity is up to 17 bits at the data rate of 100 Gbps. The propagation path of our design is folded by up to 5 times (or 10 times for the one-port design) as compared to the conventional optical buffers using the direct fiber delay lines. The footprint of the device is 10 mm × 0.5 mm, and 20 of them can be fit into the area of about 1cm². By further optimization of the design parameters, a longer time delay can be expected by suppressing the dispersion and the loss. This design may be useful for optical buffering and signal processing in all-optical networks and optical computing.

REFERENCES

[1]   G. Garzoglio, P. Mhashilkar, H. Kim, D. Dykstra, and M. Slyz, "Big data over a 100G network at Fermilab," J. Phys. Conf. Ser., vol. **513**, pp. 062017, 2014.

[2]   N. Beheshti, E. Burmeister, Y. Ganjali, J. E. Bowers, D. J. Blumenthal, and N. McKeown, "Optical packet buffers for backbone Internet routers," IEEE/ACM Trans. Netw., vol. **18**, pp. 1599–1609, 2010.

[3]   E. F. Burmeister, D. J. Blumenthal, and J. E. Bowers, "A comparison of optical buffering technologies," Opt. Switch. Netw., vol. **5**, pp. 10–18, 2008.

[4]   R. S. Tucker, "The role of optics and electronics in high-capacity routers," J. Light. Technol., vol. **24**, pp. 4655–4673, 2006.

[5]   T. Baba, "Slow light in photonic crystals," Nat. Photonics, vol. **2**, pp. 465–473, 2008.

[6]   H. Takesue, N. Matsuda, E. Kuramochi, W. J. Munro, and M. Notomi, "An on-chip coupled resonator optical waveguide single-photon buffer.," Nat. Commun., vol. **4**, pp. 2725, 2013.

[7]   E. Kuramochi, K. Nozaki, A. Shinya, K. Takeda, T. Sato, S. Matsuo, H. Taniyama, H. Sumikura, and M. Notomi, "Large-scale integration of wavelength-addressable all-optical memories on a photonic crystal chip," Nat. Photonics, vol. **8**, pp. 474–481, 2014.

[8]   J. B. Khurgin, "Optical buffers based on slow light in electromagnetically induced transparent media and coupled resonator structures: comparative analysis," J. Opt. Soc. Am. B, vol. **22**, pp. 1062–1074 , 2005.

[9]   R. S. Tucker, P. C. Ku, and C. J. Chang-Hasnain, "Slow-light optical buffers: Capabilities and fundamental limitations," J. Light. Technol., vol. **23**, pp. 4046–4066, 2005.

[10]   Q. Xu, P. Dong, and M. Lipson, "Breaking the delay-bandwidth limit in a photonic structure," Nat. Phys., vol. **3**, pp. 406–410, 2007.

[11]   H. Yum, X. Liu, Y. J. Jang, M. E. Kim, and S. M. Shahriar, "Pulse delay via tunable white light cavities using fiber-optic resonators," J. Light. Technol., vol. **29**, pp. 2698–2705, 2011.

[12]   J. Scheuer and M. S. Shahriar, "Trap-door optical buffering using a flat-top coupled microring filter: the superluminal cavity approach," Opt. Lett., vol. **38**, pp. 3534–3537, 2013.

[13]   J. J. Xiao, J. T. A. Kwok, and K. W. Yu, "Light trapping and releasing in side-coupled microresonator structures with asymmetric cavity–waveguide coupling," Opt. Commun., vol. **281**, pp. 4023–4027, 2008.

[14]   H. Park, J. P. Mack, D. J. Bluementhal, and J. E. Bowers, "An integrated recirculating optical buffer," Opt. Express, vol. **16**, pp. 11124–11131, 2008.

[15]   E. F. Burmeister, J. P. Mack, H. N. Poulsen, M. L. Masanović, B. Stamenić, D. J. Blumenthal, and J. E. Bowers, "Photonic integrated circuit optical buffer for packet-switched networks," Opt. Express, vol. **17**, pp. 6629–6635, 2009.

[16]   H. Lee, T. Chen, J. Li, O. Painter, and K. J. Vahala, "Ultra-low-loss optical delay line on a silicon chip," Nat. Commun., vol. **3**, pp. 867, 2012.

[17]   M. Yamaguchi and K. Hirabayashi, "Variable optical delay line based on a birefringent planar optical platform," Opt. Lett., vol. **20**, pp. 644–646, 1995.

[18]   T. Pertsch, T. Zentgraf, U. Peschel, a. Bräuer, and F. Lederer, "Beam steering in waveguide arrays," Appl. Phys. Lett., vol. **80**, pp. 3247–3249, 2002.

[19]   D. N. Christodoulides, F. Lederer, and Y. Silberberg, "Discretizing light behaviour in linear and nonlinear waveguide lattices," Nature, vol. **424**, pp. 817–823, 2003.

[20]   M. Kuznetsov, "Coupled wave analysis of multiple waveguide systems: The discrete harmonic oscillator," IEEE J. Quantum Electron., vol. **21**, pp. 1893–1898, 1985.

[21]   R. Gordon, "Harmonic oscillation in a spatially finite array waveguide," Opt. Lett., vol. **29**, pp. 2752–2754, 2004.

[22]   J. Wu, A. Joushaghani, and J. S. Aitchison, "Harmonic oscillation in coupled waveguide arrays," in 2014 Conf. on Lasers and Electro-Optics (CLEO). San Jose, CA: IEEE, pp. 1-2.

[23]   J. Wu, "Harmonic oscillations in optical waveguide arrays," M.S. Thesis, Dept. Electr. & Comput. Eng., Univ. Toronto, Toronto, Canada, 2013.

[24]   R. Morandotti, U. Peschel, J. S. Aitchison, H. S. Eisenberg, and Y. Silberberg, "Experimental observation of linear and nonlinear optical bloch oscillations," Phys. Rev. Lett., vol. **83**, pp. 4756–4759, 1999.

[25]   T. Pertsch, P. Dannberg, W. Elflein, A. Bräuer, and F. Lederer, "Optical Bloch oscillations in temperature tuned waveguide arrays," Phys. Rev. Lett., vol. **83**, pp. 4752–4755, 1999.

[26]   M. J. Zheng, Y. S. Chan, and K. W. Yu, "Harmonic oscillations and their switching in elliptical optical waveguide arrays," J. Opt., vol. **13**, pp. 035708, 2011.

[27]   M. J. Zheng, Y. S. Chan, and K. W. Yu, "Steering between Bloch oscillation and dipole oscillation in parabolic optical waveguide arrays," J. Opt. Soc. Am. B, vol. **27**, pp. 1299–1304, 2010.

[28]   S. Longhi, "Dynamic trapping of light in modulated waveguide lattices," Opt. Lett., vol. **36**, pp. 819–821, 2011.

[29]   N. B. Plougonven, C. Minot, G. Bouwmans, A. Levenson, and J.-M. Moison, "Discrete photonics resonator in coupled waveguide arrays," Opt. Express, vol. **22**, pp. 12379–12391, 2014.

[30]   J. K. S. Poon, P. Chak, J. M. Choi, and A. Yariv, "Slowing light with Fabry-Pérot resonator arrays," J. Opt. Soc. Am. B, vol. **24**, 2763–2769, 2007.

[31]   J. Scheuer, J. Poon, G. Paloczi, A. Yariv, "Coupled resonator optical waveguides (CROWs)," Adv. Opt. Quantum Mem. Comput. II, vol. **5735**, 52–59, 2005.

[32]   Y. Li, Y. Xi, X. Li, and W.-P. Huang, "Design and analysis of single mode Fabry-Pérot lasers with high speed modulation capability," Opt. Express, vol. **19**, pp. 12131–12140, 2011.

[33]   M. G. Davis and R. F. O'Dowd, "A new large-signal dynamic model for multielectrode DFB lasers based on the transfer matrix method," IEEE Photonics Technol. Lett., vol. **4**, pp. 838–840, 1992.

[34]   P. Morel and a Sharaiha, "Wideband Time-Domain Transfer matrix model equivalent circuit for short pulse propagation in semiconductor optical amplifiers," IEEE J. Quantum Electron., vol. **45**, pp. 103–116, 2009.

[35]   A. Ghatak and K. Thyagarajan, *An Introduction to Fiber Optics*. New York: Cambridge Unviersity Press, 1998, pp. 83–84,.

[36]   K. Okamoto, *Fundamentals of Optical Waveguides. New York:* Academic Press, 2006, pp. 13–207.

[37]   Y. Zhao, C. Argyropoulos, and Y. Hao, "Full-wave finite-difference time-domain simulation of electromagnetic cloaking structures," Opt. Express vol. **16**, 6717–6730, 2008.

Tenghao Li received B. Eng. in mechanical engineering and M. Eng. in optical engineering from Tsinghua University, Beijing, China, in 2011 and 2014, respectively. He is currently working toward the Ph.D. degree on electro-optic devices in Department of Applied Physics, The Hong Kong Polytechnic University.

Qingming Chen received B.S. in optical information science and technology from the Huazhong University of Science and Technology, Wuhan, China, in 2011, and M.Eng. in optical engineering from Jinan university, Guangzhou, China, in 2014. He is currently a PhD candidate in the Hong Kong Polytechnic University. His research include optofluidics and photonics.

Yunfeng Xiao received the B.S. and Ph.D. degrees in physics from University of Science and Technology of China in 2002 and 2007, respectively. After a postdoctoral research at Washington University in St. Louis, he joined the faculty of Peking University in 2009, and was promoted to Associate Professor with tenure in 2014. His research focuses on microcavity optics and photonics.

Xuming Zhang received B.Eng. in precision mechanical engineering from the University of Science and Technology of China, in 1994, and Ph.D. in Electronic Engineering from Nanyang Technological University, Singapore, in 2006. He is currently an Associate Professor with Hong Kong Polytechnic University. His research interests cover micro-/nano-optics, microfluidics, sensors and photocatalysis.